Dynamical model of birdsong maintenance and control

Henry D. I. Abarbanel*
Department of Physics and Marine Physical Laboratory, Scripps Institution of Oceanography, La Jolla, California 92093-0233, USA

Sachin S. Talathi†
Department of Physics and Institute of Nonlinear Science, University of California–San Diego, La Jolla, California 92093-0402, USA

Gabriel Mindlin and Misha Rabinovich
Institute for Nonlinear Science, University of California–San Diego, La Jolla, California 92093-0402, USA

Leif Gibb
Graduate Program in Computational Neurobiology, and Institute for Nonlinear Science, Division of Biological Sciences, University of California–San Diego, La Jolla, California 92093-0402, USA
(Received 7 March 2004; published 22 November 2004)

The neuroethology of song learning, production, and maintenance in songbirds presents interesting similarities to human speech. We have developed a biophysical model of the manner in which song could be maintained in adult songbirds. This model may inform us about the human counterpart to these processes. In songbirds, signals generated in nucleus High Vocal center (HVc) follow a direct route along a premotor pathway to the robust nucleus of the archistriatum (RA) as well as an indirect route to RA through the anterior forebrain pathway (AFP): the neurons of RA are innervated from both sources. HVc expresses very sparse bursts of spikes having interspike intervals of about 2 ms. The expressions of these bursts arrive at the RA with a time difference $\Delta T \approx 50 \pm 10$ ms between the two pathways. The observed combination of AMPA and NMDA receptors at RA projection neurons suggests that long-term potentiation and long-term depression can both be induced by spike timing plasticity through the pairing of the HVc and AFP signals. We present a dynamical model that stabilizes this synaptic plasticity through a feedback from the RA to the AFP using known connections. The stabilization occurs dynamically and is absent when the RA $\rightarrow$ AFP connection is removed. This requires a dynamical selection of ΔT. The model does this, and ΔT lies within the observed range. Our model represents an illustration of a functional consequence of activity-dependent plasticity directly connected with neuroethological observations. Within the model the parameters of the AFP, and thus the magnitude of ΔT, can also be tuned to an unstable regime. This means that destabilization might be induced by neuromodulation of the AFP.

DOI: 10.1103/PhysRevE.70.051911 PACS number(s): 87.17.Aa, 87.16.Ac

I. INTRODUCTION

Learning and maintenance of song in songbirds present interesting questions about the basic biological physics of birdsong. The study of the detailed mechanism and neurophysiology of the collection of neurons, called nuclei, constituting the song system of songbirds might also inform one's interest in the human speech counterpart of song [1]. Each nucleus consists of the order of 10 000 neurons and is not homogeneous in its neural composition. Some detail about the properties of neurons in each nucleus has been revealed by electrophysiological experiments in the past decade, and we shall review this information as we develop the model discussed in this paper. Despite the inhomogeneity in each nucleus, the birdsong nuclei in the premotor pathway and the nuclei of the anterior forebrain pathway, which is closely linked with it, appear to act in a cooperative manner with regard to the timing of signals observed during song production [2].

Production of song directly involves the premotor pathway from the nucleus High Vocal center (HVc) (used as a proper name) to the robust nucleus of the archistriatum (RA) and then from the RA by projection through the tracheosyringeal portion of the hypoglossal nucleus to the syrinx muscles controlling tension in the nonlinear song membrane and through the nucleus ambiguus and nucleus retroambigualis to the motorneurons controlling respiratory action in the songbox. The balance between the timing of tension signals and respiratory signals is thought to control the quality and details of song production [3,4]. From vocalization in the songbox there is auditory feedback which plays a critical role in maintaining song, although the neural correlates of this auditory pathway remain poorly understood [5].

The knowledge of the neural nuclei involved in song production and maintenance has been well reviewed in several places [6–8]. In Fig. 1 we illustrate the main nuclei involved in both the direct premotor pathway from the HVc to the RA and the indirect connection through the anterior forebrain pathway (AFP) composed of the nuclei area X, which receives input directly from HVc, the medial nucleus of the dorsolateral thalamus (DLM), which acts as an important relay station receiving inhibition from area X, and the lateral part of the magnocellular nucleus of the anterior neostratum

*Also at Institute for Nonlinear Science, University of California–San Diego, La Jolla, CA 92093-0402, USA.
†Electronic address: talathi@physics.ucsd.edu

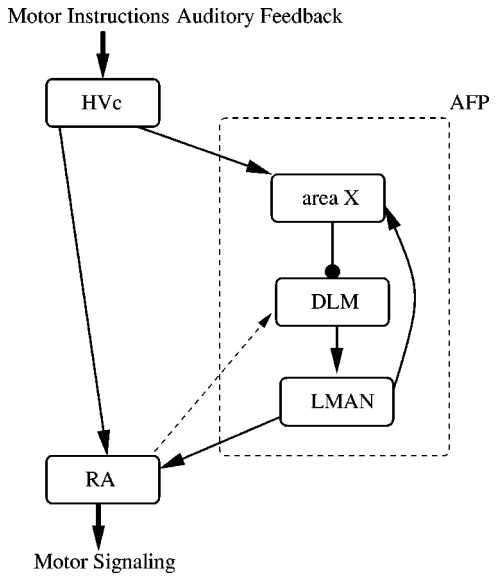

FIG. 1. Diagram of the premotor pathway, HVc and RA nuclei, and the anterior forebrain pathway, AFP, comprised of area X, DLM, and LMAN. HVc receives motor instructions which are expressed as sparse bursts to the RA and to area X. The AFP is a control and maintenance pathway. Signals from HVc through the AFP arrive at the RA with a time delay $\Delta T \approx 50 \pm 10$ ms. The arrows at the end of lines represent excitatory couplings; the filled circles, inhibitory coupling. The dotted line is a known connection between RA and DLM whose physiological properties are not yet established.

(LMAN), which receives input from the DLM and projects both to area X and, as the AFP output, to RA. In addition we show in a dashed line the known, but unexplored, connection from the RA to the DLM which will play a role below.

The AFP is known to be important in song development during the sensory learning period when the juvenile bird listens to its tutor and is presumed to make a neural template of its tutor's song. It is also important in the sensorimotor learning phase when the bird listens to his own song and perfects it to resemble the tutor's instructions. If the AFP is lesioned during these periods, completion of learning, called crystallization, occurs prematurely with only poor quality song resulting. If the AFP is lesioned in an adult, following crystallization of song, the song remains relatively stable. If the bird is deafened as an adult, song slowly degenerates, but simultaneous lesioning of the LMAN prevents this degeneration [9]. This suggests, as noted in [5], that the AFP processes input from the HVc to provide a signal to the RA which can be variable and sculpting of song in the juvenile, while retaining a role in maintaining adult song.

Experiments on the action of HVc neurons projecting to the RA along the premotor pathway show that each HVc neuron fires sparsely, once every motif in a song or about once every 1000 ms, and during this burst of activity produces 4.5 ± 2 spikes in a time lasting 6.1 ± 2 ms [10]. HVc also projects processes to area X, and the evidence is that this signaling is also sparse with, perhaps, three times the frequency of short bursts observed going to the RA.

The RA acts primarily as a "junction box" processing, in a one-to-many fashion, elementary signals from HVc$\rightarrow$RA projection neurons and gathering collections of these signals into population organized instruction signals to the syrinx and to the respiratory system for song production. In this paper we will suggest another role for the RA, namely, conveying through a closed feedback loop information about the timing of signals it receives from the HVc and the AFP and using this information to direct maintenance of song developed in the sensorimotor phase of learning.

Observations by Kimpo, Doupe, and Theunissen [2] have demonstrated that neural activity from the output nucleus of the AFP, LMAN, and from RA activity has two correlation peaks: one is associated with action in the LMAN occurring about 10 ms before it arrives by a known neural pathway to the RA, and the other is associated with direct action from HVc arriving at the RA followed by a delay of order 50 ± 10 ms associated with the time to traverse the AFP. This result is remarkable as it shows that the coordinated action of the AFP maintains precise timing information about HVc signals even though the signal must pass through several stations of neural action, namely, area X, then the DLM, and then the LMAN, each of which will involve unreliable synaptic firing.

The measurements of [2] suggest both that timing is critical in the operation of the song system, shown in Fig. 1, and that the nuclei in the AFP though composed of numerous, unreliable components might be seen as a coherent, coordinated dynamical system in terms of its role in timing of neural signals to the RA.

In this paper we investigate this picture of the song system using the important approximation that cell types in each nucleus, to the extent they are known, can be represented by a small number of excitable nonlinear oscillators represented by conductance based Hodgkin-Huxley (HH) neurons. We will treat HVc as a fundamental signal generator. It will initiate, in a manner not addressed here, sparse bursts of high frequency (613 ± 210 Hz) spikes projecting to the RA and area X. The RA processes these sparse bursts in a fashion we have explored elsewhere [11], while the AFP relays these sparse bursts to the RA producing a time delay ΔT whose biophysical origin we will explore.

Using observations on the neural structure of the RA [12,13] and the distribution of AMPA and NMDA glutamate receptors, which are ligand gated ion channels, named after the agonist that activates them, NMDA (N-methyl-D-asparate) and AMPA (α-amino-3-hydroxyl-5-methyl-4-isoxazole-propionate) at the RA [14] along with our previously explored biophysical model for synaptic plasticity at AMPA receptors [15], we will investigate the change in AMPA channel strength as a function of ΔT showing that $\Delta T \approx 50$ ms is a region where the change in synaptic strength is nearly zero.

Then we will examine the biophysical origins of ΔT in our model of the AFP and show that such a ΔT is attributable to the nature of the inhibition in area X and in its projections to the DLM. Finally, to connect the apparent utility of $\Delta T \approx 40$ ms at RA neurons in a stabilized song and the dynamically determined ΔT in the AFP, we suggest properties for the known RA$\rightarrow$DLM connection which would stabilize the complete HVc, RA, AFP system. The connection we propose has not been explored electrophysiologically, and we make

suppositions as to its properties. It can be tested in detail experimentally. It provides one way in which the plasticity in the RA needed for development of song instructions in the premotor pathway can be informed of the timing in the AFP. We will demonstrate that there are regions of parameters in the AFP network where the full system is stable and could be the source of stable maintenance of the song, and regions where the strength of the HVc→RA AMPA connections is systematically but reversibly weakened permitting the development of other song patterns. Neuromodulators, such as dopamine, may play a role in dictating which regime is selected in various stages of songbird development [16,17].

Our plasticity model [15] was developed in the context of the small observed changes in AMPA conductivity seen in a variety of experiments [18]. There is neither a saturation at high values of the conductivity nor a lower bound at zero conductivity built into the model, though one could clearly do that mathematically [19]. The biological physics of the synaptic strength changes come from the requirement that the conductivity be greater than or equal to zero, and that the resources, "silent" AMPA receptors or other biochemical ingredients [20,21], in the processes leading to conductivity augmentation are bounded.

The synaptic plasticity model we use here does not have these features. Nonetheless, the feedback coupling we identify allowing the AFP to know what ΔT is experienced by synapses at the RA nucleus leads to finite AMPA conductivity at the HVc→RA synapses. Removing this feedback leads to unbounded growth in the AMPA conductivity in our model. This dynamical stability mechanism may be operating in feedback loops in other neural systems. Since this stability is quite robust to the parameters of the model, in particular to the changes in the excitatory and inhibitory couplings in the network, the principle of stability through feedback in neural networks could have broad application.

The model we develop here for the premotor (RA and HVc) nuclei and the AFP (area X, DLM, and LMAN) nuclei uses conductance based HH models for each node of the network and simplified neurotransmitter dynamics at each connection. We have done our best to reproduce the synaptic and intrinsic currents known from a variety of experimental observations, and this results in a somewhat complex model for the system we study. It is interesting to ask if all this could be simplified. It is likely that we could have used rather simpler spiking neural models at most locations in our network as many of the HH neurons need only have the ability to produce action potentials to play their role in the dynamics studied here. However, in at least one instance, namely, the detailed dynamics of response in the DLM nucleus, the role of the internal variables of a HH model, namely, the activation and inactivation dynamics, performs a key task in determining the timing of signal propagating around the AFP. These internal dynamical variables are absent in most simplified spiking neural models. We have chosen, therefore, to present here a model where the full set of ionic and synaptic currents, as we know them from observations, are represented, allowing the internal dynamics to unfold where required and providing a model with a uniform representation of the nuclei in the song system. The details of the currents and the synaptic plasticity model are presented in an Appendix while the dynamics of the system will be developed now.

II. THE RA NUCLEUS: STRUCTURE AND PLASTICITY

In this section we first discuss the neural structure of the RA nucleus and our representation of that structure. Then we recall our model of synaptic plasticity [15] and apply it to the particular distribution of AMPA and NMDA receptors observed to be present in the adult zebra finch [14].

A. RA structure

The RA nucleus acts in the main as a "junction box" translating the sparse signals from each RA projecting HVc neuron into instructions to the nonlinear tension of muscles in the syrinx and to the respiratory pressure from the lungs. The correlated application of tension and pressure to the songbox has been shown to be the key driving signals to the songbox in the production of song vocalization [3,4].

Spiro, Dalva, and Mooney [12] have examined the electrophysiology of neuron types in the RA nucleus. They identified a class of interneurons (INs) which are distinguished morphologically as well as electrophysiologically from RA projection neurons (PNs). The PNs and the INs receive excitatory projections both from HVc along the premotor pathway and from LMAN as the output from the AFP. The INs also receive excitatory inputs from the PNs, and the INs, in turn, provide long range GABAergic inhibition to populations of RA PNs. These populations of PNs project to different sets of motor nuclei which coordinate the respiratory pressure and the nonlinear tension of muscles in the syrinx.

In the absence of input from HVc, and thus from the LMAN as its activity is induced by HVc signals into the AFP, the INs are at a resting potential of about -66 ± 3 mV [12]. In the same setting, the PNs are firing nearly periodically at about 15–30 Hz. There is also reported to be a weak mutual excitatory connection among the PNs having their efferents onto the same type of motor nuclei [22]. These connections are weak enough that the PNs appear not to be synchronized. When a burst from HVc arrives at the RA, the INs are activated and inhibit the low frequency oscillations of the PNs and allow the PNs to be entrained by the high frequency signal from HVc. This results in a temporally more precise pattern of PN firing, and this is relayed to vocal and respiratory neural nuclei. The PNs outnumber the INs in RA by an estimated ratio of 30:1.

Our model of the RA nucleus internal structure is shown in Fig. 2 where we have two PNs and one IN to represent the nucleus. A larger model with order of 100 PNs projecting to muscle control and 100 PNs projecting to respiration control along with 3–5 PNs in each population would be required to represent the way the RA nucleus distributes command signals from many HVc RA projecting neurons and determines details of syllables in each motif of a song [11]. Our focus here is in the mechanisms which control the synaptic plasticity at the HVc→RA junctions, and what we reveal in our calculations will be operating at each such junction in a larger model. We do not develop a model of song production

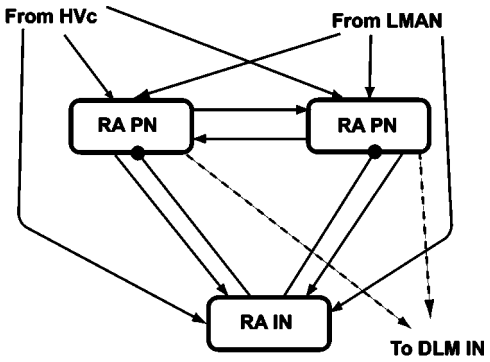

FIG. 2. The structure of the RA nucleus in our model. RA projection neurons (PNs) receive input from both HVc and, through the AFP, from the LMAN. RA-PNs are coupled with weak excitation. Populations of RA-PNs project to the syrinx and to the control of the respiratory system. RA interneurons (INs) also receive input from both HVc and LMAN. They receive excitatory signals from the PNs and project back inhibitory couplings. The arborization of the PNs is broad, and it is estimated that the ratio of PNs:INs is about 30:1 [12]. Here we represent the RA nucleus with two PNs and one IN. When there is no song input from HVc directly or via the AFP, the PNs are at rest and the INs oscillate at about 15–30 Hz. The output to DLM interneurons is shown in dotted lines. The arrows at the end of lines represent excitatory couplings; the filled circles represent inhibitory coupling.

here, encompassing a discussion of the full matrix of one-to-many HVc→RA connections. Our goal is to understand the dynamics of the synaptic plasticity which can provide stable connections for the fully developed matrix of connections in adult songbirds. Our exploration of the song production through stabilized, and thus fixed over the short-term of song production, HVc→RA connections is in [11].

B. RA-PNs

The dynamics of the membrane voltage of the jth RA-PN, $V_{RA\text{-}PNj}(t)$, is given by ($j=1,2,\ldots,N_{RA}$; $N_{RA}=2$ here) a standard HH conduction based neuron model along with synaptic currents associated with the other network connections (see Fig. 2):

$$\begin{aligned} C_M\frac{dV_{RA\text{-}PNj}(t)}{dt} &= I_{HH}(t,V_{RA\text{-}PNj}(t)) + I_{HVc\text{-}NMDA}(t,V_{RA\text{-}PNj}(t)) \\ &+ I_{HVc\text{-}AMPA}(t,V_{RA\text{-}PNj}(t)) \\ &+ I_{LMAN\text{-}NMDA}(t,V_{RA\text{-}PNj}(t)) \\ &+ I_{LMAN\text{-}AMPA}(t,V_{RA\text{-}PNj}(t)) + I_{DC\text{-}PNj} \\ &+ I_{IN\to PNj}(t,V_{RA\text{-}PNj}(t)) \\ &+ I_{PN\to PNj}(t,V_{RA\text{-}PNj}(t)), \end{aligned} \tag{1}$$

where C_M is the membrane capacitance, and the intrinsic HH currents are

$$\begin{aligned} I_{HH}(t,V(t)) &= g_{Na}m(t)^3h(t)[E_{Na}-V(t)] + g_Kn(t)^4[E_K-V(t)] \\ &+ g_L[E_L-V(t)]. \end{aligned} \tag{2}$$

g_{Na}, g_K, and g_L are the maximal conductances of the sodium, potassium, and leak channels, respectively, and the $E_{\cdot}$ are reversal potentials. All parameter values not specifically mentioned in the text are listed in the Appendix.

The activation and inactivation variables $Y(t)=m(t),h(t),n(t)$ satisfy first-order kinetic equations

$$\frac{dY(t)}{dt} = \nu[\alpha_Y(V(t))[1-Y(t)] - \beta_Y(V(t))Y(t)], \tag{3}$$

where $\nu=10$ and,

$$\begin{aligned} \alpha_m(V) &= \frac{-0.32(52+V)}{e^{-(V+52)/4}-1}, \quad \beta_m(V) = \frac{0.28(25+V)}{e^{(V+25)/5}-1}, \\ \alpha_h(V) &= 0.128e^{-(V+48)/18}, \quad \beta_h(V) = \frac{4}{e^{-(V+25)/5}+1}, \\ \alpha_n(V) &= \frac{-0.032(50+V)}{e^{-(V+50)/5}-1}, \quad \beta_n(V) = 0.5e^{-(55+V)/40}, \end{aligned} \tag{4}$$

and all voltages are in millivolts. This choice of dynamics is discussed in the Appendix.

$I_{DC\text{-}PNj}$ is a dc current injected into the RA-PNs. It is set so the autonomous oscillation frequency of the RA-PNs is 15–20 Hz.

The synaptic current due to HVc signals stimulating glutamate to arrive at NMDA receptors is

$$\begin{aligned} I_{HVc\text{-}NMDA}(t,V(t)) &= \frac{g_N}{2}S_{N\text{-}HVc}(t,V_{HVc}(t))B(V(t)) \\ &\times[E_{rev}-V(t)], \end{aligned} \tag{5}$$

where g_N is a maximal conductance, and $B(V)$ is the block of the NMDA receptor [23,24] due to extracellular magnesium ions having concentration $[Mg^{2+}]$

$$B(V) = \frac{1}{1+0.288[Mg^{2+}]e^{-0.062V}}, \tag{6}$$

and $V_{HVc}(t)$ is the voltage of the signal arriving from HVc.

$E_{rev}=0$ mV is the reversal potential of the excitatory NMDA synapse, and $S_{N\text{-}HVc}(t,V(t))$ represents the fraction of open NMDA receptor channels on the postsynaptic RA-PN. To achieve the time course of this process on NMDA receptors we use a two-component form for $S_{N\text{-}HVc}(t,V(t))$:

$$\begin{aligned} S_{N\text{-}HVc}(t,V(t)) &= w_{HVc}S_{N1\text{-}HVc}(t,V(t)) + (1 \\ &- w_{HVc})S_{N2\text{-}HVc}(t,V(t)), \end{aligned} \tag{7}$$

where the $S_{Nl\text{-}HVc}(t,V(t))$ $l=1,2$ satisfy

$$\frac{dS_{Nl\text{-}HVc}(t,V(t))}{dt} = \frac{1}{\tau_{Nl\text{-}HVc}}\frac{S_0(V_{pre})-S_{Nl\text{-}HVc}(t,V(t))}{S_{1Nl\text{-}HVc}-1}, \tag{8}$$

and $S_0(V_{pre})$ is a step function in voltage which rises rapidly from its value of 0, before an action potential appears in the presynaptic terminal, to 1 as the action potential arrives, then

falls rapidly back to 0. We represent it in our modeling by

$$S_0(V_{pre}) = 0.5\{1 + \tanh[120(V_{pre} - 0.1)]\}, \tag{9}$$

with V_{pre} being scaled between 0 and 1 representing arrival of presynaptic spike. $\tau_{Nl\text{-}HVc}$ and $S_{1nl\text{-}HVc}$ are two constants determining the docking and undocking of neurotransmitters represented by $S_{Nl\text{-}HVc}(t, V(t))$: the neurotransmitter docks with a time constant $\tau_{Nl\text{-}HVc}(S_{1nl\text{-}HVc} - 1)$ and undocks with a time constant $\tau_{Nl\text{-}HVc}S_{1nl\text{-}HVc}$.

This two-component model is based on observations by Stark and Perkel [14] who recorded NMDA currents in zebra finches of several different age groups, including adults. They fitted these currents with a double exponential decay function and reported fast and slow time constants and the percentage contribution of the slow component. To reflect these measurements we use two processes with different decay time constants. Their measured values for the fast component at HVc-RA synapses were 20 ± 7.8 ms and 100 ± 56 ms for the slow component. The slow component was $(68 \pm 11)\%$ of the current. For LMAN-RA NMDA synapses, they observed fast and slow time constants of 30 ± 8.6 ms and 140 ± 55 ms, respectively, and $(59 \pm 4.9)\%$ slow component.

The synaptic current due to HVc projections to the RA associated with AMPA receptors $I_{HVc\text{-}AMPA}(t, V_{RA\text{-}PNj}(t))$ is given by

$$I_{HVc\text{-}AMPA}(t, V(t)) = g_{RA}(t)S_A(t, V_{HVc}(t))[E_{rev} - V(t)], \tag{10}$$

where $g_{RA}(t)$ is the plastic, time-dependent AMPA conductivity determined by our synaptic plasticity dynamics as given below, and $S_A(t, V(t))$ represents the fraction of open AMPA receptors on the postsynaptic RA-PN. It satisfies

$$\frac{dS_A(t, V(t))}{dt} = \frac{1}{\tau_A}\frac{S_0(V_{pre}) - S_A(t, V(t))}{S_{1A} - 1}. \tag{11}$$

In our model we have taken $\tau_A = 1.4$ ms and $S_{1A} = 15/14$ leading to a glutamate docking time constant of 0.1 ms and an undocking time constant of 1.5 ms.

The synaptic current due to LMAN signals at NMDA receptors is

$$I_{LMAN\text{-}NMDA}(t, V(t)) = g_N S_{N\text{-}LMAN}(t, V_{LMAN}(t))B(V(t)) \times [E_{rev} - V(t)]. \tag{12}$$

$S_{N\text{-}LMAN}(t, V(t))$ represents the fraction of glutamate docked on the NMDA receptors of the postsynaptic RA-PN. To achieve the time course of this process on NMDA receptors we use a two-component form for $S_{N\text{-}LMAN}(t, V(t))$:

$$S_{N\text{-}LMAN}(t, V(t)) = (1 - w_{LMAN})S_{N2\text{-}LMAN}(t, V(t)) + w_{LMAN}S_{N1\text{-}LMAN}(t, V(t)), \tag{13}$$

where the $S_{Nl\text{-}LMAN}(t, V(t))l = 1,2$ satisfy

$$\frac{dS_{Nl\text{-}LMAN}(t, V(t))}{dt} = \frac{1}{\tau_{Nl\text{-}LMAN}}\frac{S_0(V_{pre}) - S_{Nl\text{-}LMAN}(t, V(t))}{S_{1Nl\text{-}LMAN} - 1}. \tag{14}$$

$\tau_{Nl\text{-}LMAN}$ and $S_{1nl\text{-}LMAN}$ are two constants determining the docking and undocking of the neurotransmitter represented by $S_{Nl\text{-}LMAN}(t, V(t))$: the neurotransmitter docks with a time constant $\tau_{Nl\text{-}LMAN}(S_{1nl\text{-}LMAN} - 1)$ and undocks with a time constant $\tau_{Nl\text{-}LMAN}S_{1nl\text{-}LMAN}$.

In our model we have chosen $w_{HVc} = 0.21$, $w_{LMAN} = 0.41$, $\tau_{N1\text{-}HVc} = 19.75$ ms, $\tau_{N2\text{-}HVc} = 99.75$ ms, $S_{N1\text{-}HVc} = 20/19.75$, $S_{N2\text{-}HVc} = 100/99.75$, $\tau_{N1\text{-}LMAN} = 29$ ms, $\tau_{N2\text{-}LMAN} = 139$ ms, $S_{N1\text{-}LMAN} = 30/29$, and $S_{N2\text{-}LMAN} = 140/139$.

The synaptic current due to LMAN projections to the RA associated with AMPA receptors $I_{LMAN\text{-}AMPA}(t, V_{RA\text{-}PNj}(t))$ is given by

$$I_{LMAN\text{-}AMPA}(t, V(t)) = \frac{g_{RA}(t)}{10}S_A(t, V_{HVc}(t))[E_{rev} - V(t)]. \tag{15}$$

The relative amounts of NMDA and AMPA receptors at the HVc→RA and LMAN→RA junctions are suggested by the measurements of Stark and Perkel [14].

The current $I_{IN\to PNj}(t, V_{RA\text{-}PNj}(t))$ from the IN to the jth PN is given as

$$I_{IN\to PNj}(t, V_{RA\text{-}PNj}(t)) = g_{RA\text{-}IN}S(t, V_{RA\text{-}IN}(t)) \times [E_{revI} - V_{RA\text{-}PNj}(t)], \tag{16}$$

where $g_{RA\text{-}IN}$ is a maximal conductance, and $E_{revI} = -80$ mV is the inhibitory reversal potential. $S(t, V(t))$ represents the percentage of open GABA receptors. It satisfies

$$\frac{dS(t, V(t))}{dt} = 0.15\frac{1 - S(t, V(t))}{1 + e^{-[V(t)-10]}} - 0.2275S(t, V(t)). \tag{17}$$

Finally, the synaptic current to the jth PN from other PNs is given by

$$I_{PN\to PNj}(t, V_{RA\text{-}PNj}(t)) = g_{RA\text{-}PN}\sum_{k\neq j;k=1}^{N_{RA}} S_A(t, V_{RA\text{-}PNk}(t)) \times [E_{rev} - V_{RA\text{-}PNj}(t)], \tag{18}$$

with $g_{RA\text{-}PN}$ another maximal conductance.

C. RA-INs

The RA-INs are at their resting potential when no song (signal from HVc) is expressed. The membrane voltage of the IN $V_{RA\text{-}IN}(t)$ is determined by

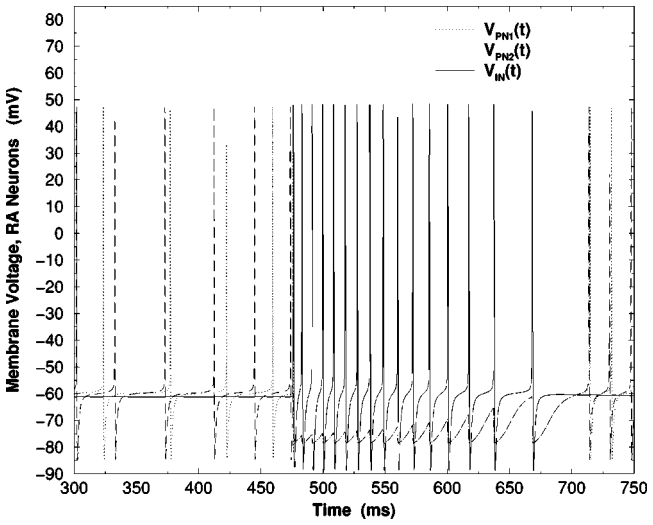

FIG. 3. Membrane voltages of neurons in the model RA nucleus. Before spikes from HVc arrive at the PN and IN cells, the IN is at rest at −61.4 mV. The PNs are oscillating autonomously at 20 Hz; they are weakly coupled by mutual excitation, but they do not synchronize. When a burst of five spikes from HVc arrives at 475 ms, the PNs are strongly inhibited and the INs begin spiking at higher frequency. As the nucleus recovers from this input, the IN oscillations decrease in frequency. About 250 ms after the arrival of the HVc signal, the nucleus recovers completely and returns to its original state.

$$C_M \frac{dV_{RA\text{-}IN}(t)}{dt} = I_{HH}(t, V_{RA\text{-}IN}(t)) + I_{HVc\text{-}NMDA}(t, V_{RA\text{-}IN}(t)) + I_{HVc\text{-}AMPA}(t, V_{RA\text{-}IN}(t)) + I_{LMAN\text{-}NMDA}(t, V_{RA\text{-}IN}(t)) + I_{LMAN\text{-}AMPA}(t, V_{RA\text{-}IN}(t)) + I_{DC\text{-}RAIN} + I_{PNj\to IN}(t, V_{RA\text{-}PNj}(t)), \quad (19)$$

with the NMDA and AMPA currents as for the RA-PNs [of course, using $V_{RA\text{-}IN}(t)$ in place of $V_{RA\text{-}PNj}(t)$] and

$$I_{PNj\to IN}(t, V_{RA\text{-}PNj}(t)) = g_{PNj\text{-}IN} S_A(t, V_{RA\text{-}PNj}) \times [E_{rev} - V_{RA\text{-}IN}(t)], \quad (20)$$

where $g_{PNj\text{-}IN}$ is the maximal conductance of the excitatory synaptic current from the RA-PN neurons to the RA-IN, and $I_{DC\text{-}RAIN}$ is a constant dc current injected into the RA-IN neuron.

This completely describes the model RA nucleus used in our work. When there is no signal from HVc or LMAN, the IN is silent at a rest potential of −61.4 mV, and the PNs are oscillating at 20 Hz. This behavior can be seen in Fig. 3. When a burst of spikes from HVc arrives (at 475 ms in Fig. 3), the PNs are strongly inhibited by the INs, while the INs oscillate at a higher frequency in response to the excitation by the burst. As the RA returns to its "rest" state, the INs slow down and return to their resting potential.

D. Plasticity in RA

The presence of AMPA and NMDA receptors on RA dendrites suggests that they will act to induce long-term potentiation or depression (LTP or LTD) through the induction of postsynaptic Ca^{2+} elevation [25]. In particular, the induction of LTP or LTD through the timing of bursts arriving from HVc and LMAN separated by ΔT suggests that mechanisms similar to those operating in spike timing plasticity [15,18] could be present here. At this time there are no direct measurements of LTP and LTD in the RA cells receiving input from HVc; however, we proceed on the assumption that the dynamics of plasticity seen elsewhere when NMDA and AMPA receptors coexist in a postsynaptic density is appropriate here.

The detailed course of biochemical pathways induced on elevating intracellular $[Ca^{2+}]$ in the postsynaptic cells is not settled at this time [26]. We have introduced a phenomenological model [15] which attempts to capture the competition known to exist in these pathways between kinases which augment AMPA conductivity by direct action on AMPA receptors or possibly by causing "silent synapses" from a store in the neuron to be placed into the postsynaptic density and phosphatases which have the opposite affect. Our model posits two intermediate phenomenological variables $P(t)$ and $D(t)$, which satisfy first-order kinetics

$$\frac{dP(t)}{dt} = f_P(\mathrm{Ca}(t) - C_0)[1 - P(t)] - \frac{P(t)}{\tau_P},$$

$$\frac{dD(t)}{dt} = f_D(\mathrm{Ca}(t) - C_0)[1 - D(t)] - \frac{D(t)}{\tau_D}, \quad (21)$$

where each variable has a driving function dependent on the departure of the intracellular Ca^{2+} concentration, $\mathrm{Ca}(t)$ from its equilibrium value $C_0 \approx 100$ nM and taken to be of the form

$$f_k(x) = \frac{x^L}{\xi^L + x^L} \quad k = P, D, \quad (22)$$

and τ_P and τ_D are time constants for the competing processes.

These auxiliary variables are then related to the change in AMPA conductivity at the RA cells via the nonlinear competition

$$\frac{1}{g_0}\frac{dg_{RA}(t)}{dt} = \gamma[P(t)D(t)^\eta - D(t)P(t)^\eta], \quad (23)$$

where g_0 is a baseline conductivity and γ and η are dimensionless constants.

The dynamics of the Ca^{2+} time course $\mathrm{Ca}(t)$ is determined by

$$\frac{d\mathrm{Ca}(t)}{dt} = \frac{C_0 - \mathrm{Ca}(t)}{\tau_C} + C_{HVc\text{-}NMDA}(t, V(t)) + C_{HVc\text{-}AMPA}(t, V(t)) + C_{LMAN\text{-}NMDA}(t, V(t)) + C_{LMAN\text{-}AMPA}(t, V(t)), \quad (24)$$

where the first term gives relaxation back to the baseline

concentration of Ca^{2+},C_0, with a time constant $\tau_C=28$ ms, and the other terms are Ca^{2+} flux terms associated with NMDA and AMPA channels as they receive signals from HVc and LMAN. The voltage $V(t)$ refers to the membrane potential of the cell where the intracellular Ca^{2+} is located.

These Ca^{2+} fluxes are

$$C_{HVc\text{-}NMDA}(t,V(t)) = g_{NC}S_{N\text{-}HVc}(t,V_{HVc}(t)) \times B(V(t))[E_{rev}-V(t)],$$

$$C_{HVc\text{-}AMPA}(t,V(t)) = g_{AC}S_A(t,V_{HVc}(t))[E_{rev}-V(t)],$$

$$C_{LMAN\text{-}NMDA}(t,V(t)) = g_{NC}S_{N\text{-}LMAN}(t,V_{LMAN}(t))B(V(t)) \times [E_{rev}-V(t)],$$

$$C_{LMAN\text{-}AMPA}(t,V(t)) = g_{AC}S_A(t,V_{LMAN}(t))[E_{rev}-V(t)]. \quad (25)$$

The intracellular voltages and the innervation from HVc and LMAN determine $Ca(t)$, and from the phenomenological model of AMPA conductance changes we determine $g_{RA}(t)$.

This model has been tested against the observations of LTP and LTD using a variety of induction protocols: spike timing [18], presentation of high frequency bursts to the presynaptic terminal [27], and action potentials presented to the presynaptic terminal when the postsynaptic neuron is depolarized at various levels [28]. To our knowledge at this time there is no direct observation of synaptic potentiation or depression at the HVc→RA junctions.

When we present a burst of five spikes with interspike intervals (ISIs) of 2 ms from HVc to this model of the RA nucleus and ΔT later present one, three, or five spikes with the same ISIs from the LMAN, we find, using our plasticity model along with the observed ratios of NMDA and AMPA receptors at the HVc and LMAN terminals [14], curves for the Δg_{RA} versus ΔT dependence such as that presented in Fig. 4. This result has $N_{HVc}=5, N_{LMAN}=5$ spikes, but the results are essentially the same for $N_{HVc}=5$ and $N_{LMAN}=1$ or 3.

The most striking feature of this result is the zero in $\Delta g_{RA}/g_0$ near $\Delta T=50$ ms. This is the order of the observed delay of signals from HVc between their direct path to the RA along a premotor route and their indirect path to the RA through the AFP. The appearance of this zero is very suggestive of a role for the AFP coupled with observed synaptic plasticity dynamics as the determinant of HVc→RA synaptic strengths. When $\Delta g_{RA}/g_0=0$, there is the opportunity for stability in these connections which would be associated with stable song since it is the instructions from HVc through these junctions in the RA that determine the population control of tension in the syrinx and the respiratory pressure. At this stage we have no way to establish the stability of this zero, but in the next sections we will address that.

There is another zero of $\Delta g_{RA}/g_0$ which is when $\Delta T \to \infty$. If one were to lesion nuclei of the AFP, this would result in this value for ΔT as no signals could traverse the AFP from HVc to reach the RA. Lesioning AFP nuclei is known to result in little change in adult birdsong, so this zero also has an attractive role in explaining observations in the song system.

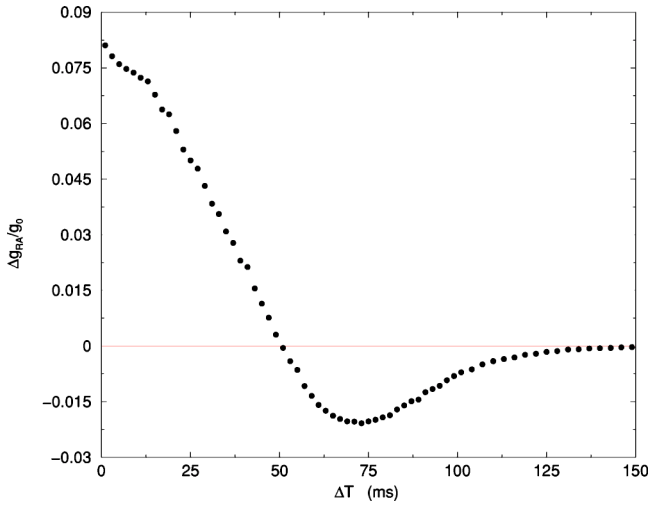

FIG. 4. Using our biophysical model of synaptic plasticity, we evaluate the change in AMPA conductivity $\Delta g_{RA}/g_0$ at the HVc→RA connections due to signals arriving from HVc followed by signals arriving from the LMAN ΔT later. In this figure the HVc signal was a burst of five spikes with interspike interval (ISI) of 2 ms. A burst of five spikes with ISI 2 ms arrives from the LMAN ΔT later. The zero in $\Delta g_{RA}/g_0$ near $\Delta T \approx 50$ ms represents potentially stable plasticity in the RA, and thus a potentially stable set of connections in the song premotor pathway. Lesions of the AFP would result in $\Delta T \to \infty$ which is also a region of $\Delta g_{RA}/g_0=0$.

III. THE AFP: STRUCTURE OF NUCLEI AND ΔT

Our model of the AFP elaborates on structure in the area X nucleus and the DLM nucleus based on observations about the excitatory and inhibitory connections within them and on electrophysiological measurements of cells in each nucleus [29–34]. Area X will be partly represented by a spiny neuron (SN) which receives the input from HVc signals. Absent these signals it is at rest. The other cell in the area X representation is an aspiny, fast firing neuron (AF) which oscillates at 15–30 Hz when there is no input from HVc. The DLM is represented by a projection neuron which receives inhibition from the AF and projects to the LMAN. There is also a DLM interneuron which receives input from the RA and in turn inhibits the DLM-PN.

A. Area X

Our representation of area X is shown in Fig. 5. Two classes of neuron are observed in area X [29,30]. We discuss them separately now.

1. The SN neuron

The SN is represented by a standard HH model with Na, K, and leak currents; a dc current is also present in the model. The SN receives input from HVc and from LMAN. The voltage of the SN $V_{SN}(t)$ is given by

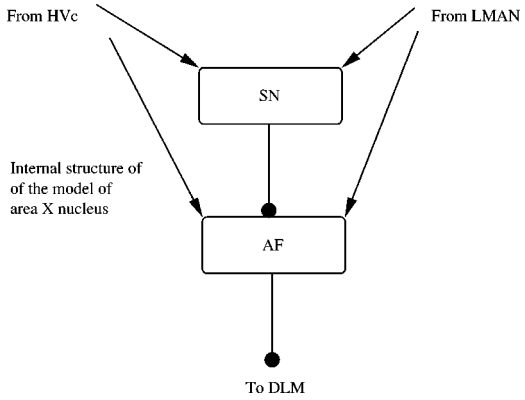

FIG. 5. The structure of the area X nucleus in our model. Spiny neurons (SNs) receive input from both HVc and LMAN. In turn the SN inhibits the aspiny, fast firing neurons (AFs). The AFs project inhibition to the DLM. When there is no song input from HVc, theSNs are at rest and the AFs oscillate at about 15–30 Hz. The arrows at the end of lines represent excitatory couplings; the filled circles, inhibitory coupling. When the AFs are active, they inhibit DLM action. On activation the SNs inhibit the AF neurons, and with the release of AF→DLM, the DLM neurons can rebound and fire. The HVc→AF connection resets the AF oscillations resulting in the SN→AF inhibition release of DLM becoming time coordinated with the arrival of a burst from HVc.

$$C_M \frac{dV_{SN}(t)}{dt} = I_{HH\text{-}AFP}(t, V_{SN}(t)) + [g_{HVc\text{-}SN} S_A(t, V_{HVc}(t)) + g_{LMAN\text{-}SN} S_A(t, V_{LMAN}(t))][E_{rev} - V_{SN}(t)] + I_{DC\text{-}SN}, \tag{26}$$

where

$$I_{HH\text{-}AFP}(t, V(t)) = g'_{Na} m_{AFP}(t)^3 h_{AFP}(t)[E'_{NA} - V(t)] + g'_K n_{AFP}((t))^4 [E'_K - V(t)] + g'_L [E'_L - V(t)] \tag{27}$$

is the familiar set of HH currents.

The activation and inactivation variables $Y_{AFP}(t) = m_{AFP}(t), h_{AFP}(t), n_{AFP}(t)$ satisfy

$$\frac{dY_{AFP}(t)}{dt} = \alpha_Y(V(t))[1 - Y_{AFP}(t)] - \beta_Y(V(t)) Y_{AFP}(t), \tag{28}$$

with

$$\alpha_{m\text{-}AFP}(V) = \frac{-0.1(35+V)}{e^{-(V+35)/10} - 1},$$

$$\beta_{m\text{-}AFP}(V) = e^{-(60+V)/18},$$

$$\alpha_{h\text{-}AFP}(V) = 0.07 e^{-(V+60)/20},$$

$$\beta_{h\text{-}AFP}(V) = \frac{1}{e^{-(V+30)/10} + 1},$$

$$\alpha_{n\text{-}AFP}(V) = \frac{-0.01(50+V)}{e^{-(V+50)} - 1},$$

$$\beta_{n\text{-}AFP}(V) = 0.125 e^{-(60+V)/80}, \tag{29}$$

and all voltages are in millivolts.

The various constants appearing here and in other sections are given in the Appendix.

2. The AF neuron

The membrane voltage $V_{AF}(t)$ of the AF neuron is determined by the standard HH ion currents plus inhibitory input from the SN and excitation from HVc and from the LMAN:

$$C_M \frac{d[V_{AF}(t)]}{dt} = I_{HH\text{-}AFP}(t, V_{AF}(t)) + g_{SN\text{-}AF} S(t, V_{SN}(t)) E_{revI} - V_{AF}(t) + I_{DC\text{-}AF} + [g_{HVc\text{-}AF} S_A(t, V_{HVc}(t)) + g_{LMAN\text{-}AF} S_A(t, V_{LMAN}(t))][E_{rev} - V_{AF}(t)], \tag{30}$$

and $I_{DC\text{-}AF}$ is chosen so that the AF neuron, absent inhibitory input from the SN, oscillates at 15–30 Hz.

B. DLM

The DLM also exhibits two classes of neuron [34]. The first, called type I by Luo and Perkel [32,34], is a projection neuron which receives inhibition from the AF in area X and projects excitation to the LMAN. It has characteristics of thalamic neurons [35,36] including indications of the presence of the current I_h. These type I cells also exhibit a high frequency sequence of action potentials when depolarized by currents of order 100 pA. Luo and Perkel show that it is probably associated with a Ca^{2+}-dependent current. They suggest one could expect this from the interaction of the low threshold Ca^{2+} current I_T with I_h; our model for the type I cells has both. In addition to the type I cells, which we call the DLM PNs, there is a type II cell, which we call the DLM INs. These do not exhibit Ca^{2+} spikes.

Our model of the DLM is illustrated in Fig. 6. The dashed line shows the RA→DLM projection we address in the next section.

1. The DLM projection neuron: Type I

This neuron is taken to satisfy the equation for its membrane voltage $V_{DLMPN}(t)$,

$$C_M \frac{V_{DLMPN}(t)}{dt} = I_{HH\text{-}AFP}(t, V_{DLMPN}(t)) + I_h(t) + I_T(t) + I_{AF\text{-}DLMPN}(t) + I_{DLMIN\text{-}DLMPN}(t) + I_{DC\text{-}DLMPN}, \tag{31}$$

where

$$I_h(t) = g_h m_h(t)[E_h - V_{DLMPN}(t)],$$

$$I_T(t) = g_T m_c(t) h_c(t) GHK[V_{DLMPN}(t)],$$

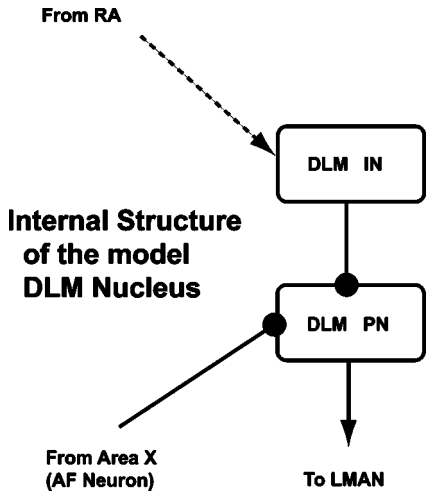

FIG. 6. The structure of the DLM nucleus in our model. The arrows at the end of lines represent excitatory couplings; the filled circles, inhibitory coupling. The DLM-PN receives inhibitory input from the area X AF neurons. It projects excitatory processes to the LMAN. In our model, input from RA excites the DLM INs which project inhibition to the DLM-PNs.

$$I_{AF\text{-}DLMPN}(t) = g_{AF\text{-}DLMPN} S(t, V_{AF}(t))[E_{revI} - V_{DLMPN}(t)],$$

$$I_{DLMIN\text{-}DLMPN}(t) = g_{DLMIN\text{-}DLMPN} S(t, V_{DLMIN}(t)) \times [E_{revI} - V_{DLMPN}(t)]. \quad (32)$$

In these expressions we have the Goldman-Hodgkin-Katz expression

$$GHK(V) = -V \frac{1 - \frac{[\mathrm{Ca}^{2+}]_o}{[\mathrm{Ca}^{2+}]_i} e^{-V/12.9}}{1 - e^{-V/12.9}}, \quad (33)$$

where the ratio of extracellular Ca^{2+}, $[Ca^{2+}]_o$, to intracellular Ca^{2+}, $[Ca^{2+}]_i$, appears. This ratio is taken to be 40 000 in our calculations.

The activation and inactivation variables $U(t) = m_h(t), m_c(t), h_c(t)$ satisfy the first-order kinetic equations

$$\frac{dU(t)}{dt} = \frac{m_{U0}(V(t)) - U(t)}{\tau_U(V(t))}, \quad (34)$$

where $V(t)$ is the membrane voltage of the cell, and, with $\tau_U(V)$ in milliseconds and V in millivolts,

$$m_{c0}(V) = \frac{1}{1 + e^{-(V+60)/6.2}},$$

$$\tau_{m_c}(V) = 0.612 + \frac{1}{e^{-(131+V)/16.7} + e^{-(16.8+V)/12.9}},$$

$$h_{c0}(V) = \frac{1}{1 + e^{(84+V)/4.03}},$$

$$\tau_{h_c}(V) = \begin{cases} e^{(467+V)/66.6} & \text{if} \quad V \leqslant -80 \quad \text{mV}, \\ 28 + e^{-(28.8+V)/10.2} & \text{if} \quad V \geqslant -80 \quad \text{mV}, \end{cases}$$

$$m_{h0}(V) = \frac{1}{1 + e^{(V+75)/5.5}},$$

$$\tau_h(V) = 0.612 + \frac{1}{e^{-(V+131.6)/16.7} + e^{(V+16.8)/18.2}}. \quad (35)$$

2. The DLM interneuron: Type II

The membrane potential $V_{DLMIN}(t)$ is taken to satisfy the ordinary HH model with synaptic currents from RA (to be explored in the next section):

$$C_M \frac{dV_{DLMIN}(t)}{dt} = I_{HH\text{-}AFP}(t, V_{DLMIN}(t)) + I_{DC\text{-}DLMIN} + I_{RA\text{-}DLMIN}(t), \quad (36)$$

with

$$I_{RA\text{-}DLMIN}(t) = g_{RA\text{-}DLMIN} \sum_{k=1}^{N_{RA}} S_A(t, V_{RA\text{-}PNk}(t)) \times [E_{revI} - V_{DLMIN}(t)]. \quad (37)$$

C. The LMAN nucleus

The membrane voltage of our LMAN nucleus $V_{LMAN}(t)$ (see Fig. 1) is represented by the HH model plus synaptic input from the DLM:

$$C_M \frac{dV_{LMAN}(t)}{dt} = I_{HH\text{-}AFP}(t, V_{LMAN}(t)) + I_{DC\text{-}LMAN} + I_{DLMPN\text{-}LMAN}(t), \quad (38)$$

with

$$I_{DLMPN\text{-}LMAN}(t) = g_{DLMPN\text{-}LMAN} S_A(t, V_{DLMPN}(t)) \times [E_{rev} - V_{LMAN}(t)]. \quad (39)$$

D. Determining ΔT

The description of the neurons in our representation of the AFP is now complete. In a realistic model of the song system one would replicate these ingredients many times over to form a larger network which has the possibility of describing the heterogeneity of the nuclei in the RA as well as the richness of the RA. Our focus in this paper is on the dynamics of each of these copies of the RA and AFP circuitry and their role in timing of signals arriving at the RA. It is in the spirit of Kimpo, Theunissen, and Doupe [2] where the nuclei of the AFP appear to act in a coherent manner in transmitting timing information about HVc bursts to the RA that we argue that our, clearly coarse grained, approximation is appropriate.

We treat the HVc nucleus as a signal generator which produces sparse bursts of spikes. The internal dynamics of the HVc is set aside now. A burst of five spikes from HVc is presented to the SN neuron in area X, and using our model of the AFP, we evaluate the time ΔT it takes for the LMAN

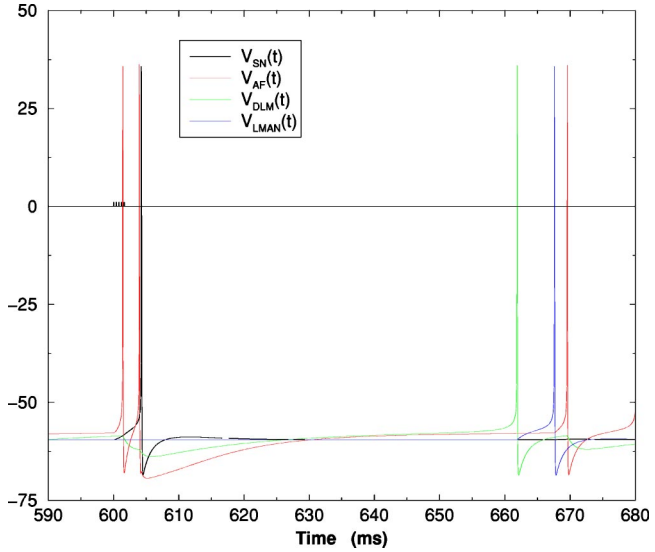

FIG. 7. The time course of membrane voltages in the AFP neurons after a burst of five spikes with ISI 2 ms arrives at SN from HVc at time 600 ms. Before the HVc burst arrives at the SN, the SN is at rest near −66 mV, and AF is oscillating at 20 Hz. AF activity inhibits the DLM projection neuron which shows small variations around rest with the same period as the AF. After the burst from HVc excites the SN, it inhibits the AF, and then the DLM recovers from its inhibition to fire about 67.5 ms later. The action potential in the DLM excites the LMAN.

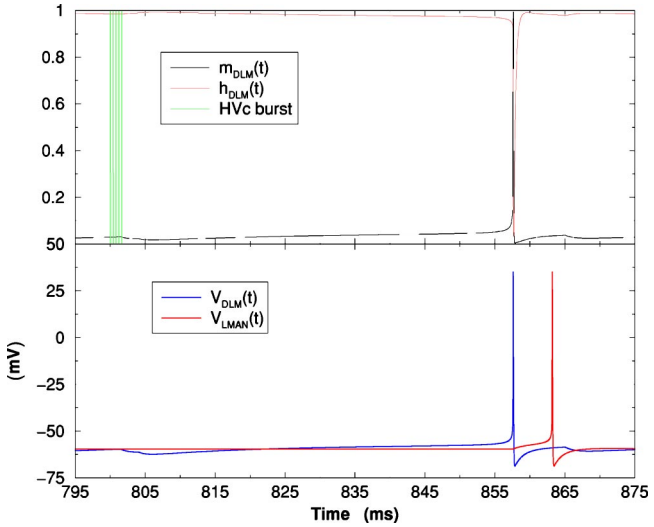

FIG. 8. Upper panel: We show the activity in the DLM-PN of the Na activation variable $m_{DLM}(t)$ and inactivation variable $h_{DLM}(t)$ following a burst of five spikes arriving at the SN (in area X) at time 800 ms. This indicates that the long time delay associated with the AFP is manifested in the slow recovery of the DLM-PN from its hyperpolariztion due to inhibition from the AF neuron in area X. When this inhibition is released, the DLM-PN responds with a spike as the activation variable slowly rises from 0 in the neuron's hyperpolarized state. Lower panel: We have the same time axis and show the membrane voltage in the DLM projection neuron and in the LMAN neuron innervated by the DLM-PN firing. The DLM-PN fires about 60 ms after the HVc burst arrives at the SN, and the LMAN neuron fires about 63 ms after the HVc burst innervates the SN.

nucleus to fire an action potential. ΔT depends on the parameters in the model AFP.

An important parameter in determining ΔT is the strength of the inhibitory connection between the AF neuron in area X and the projection neuron DLM nucleus, $g_{AF\text{-}DLMPN}$. We establish a baseline value for this in building the AFP, and then explore the ratio of this value to the baseline choice; we call this ratio $R = g_{AF\text{-}DLMPN}/g_{AF\text{-}DLMPN\text{-}Baseline}$. R is critical in our model as it is modified by the input from the RA which we introduce shortly. As input from the RA to the DLM nucleus comes through exciting the DLM interneuron which inhibits the DLM projection neuron, the strength of the RA signal effectively determines the effective strength of the inhibition of the DLM projection neuron.

By applying GABA antagonists to nucleus DLM, one can directly influence R. This suggests an experiment directly along the lines of Kimpo *et al.* [2] which measures ΔT as a function of R.

In Fig. 7 we present a typical time course for the response of the AFP following presentation of five HVc spikes with ISI of 2 ms at time 600 ms. Before these spikes arrive at the SN neuron, the AF is firing periodically at 20 Hz. This "resting" activity of the AF inhibits the DLM-PN which responds with small variations around its rest potential of ≈−65 mV. The excitation of SN by the arrival of the HVc burst inhibits AF which, in turn, releases the DLM-PN. AF is also excited by this HVc burst, and this resets the AF oscillation-effectively synchronizing the HVc arrival time and the time of inhibition of the AF by the SN. The DLM-PN then recovers from its hyperpolarized state and fires an action potential about 67 ms after the HVc burst arrives at SN followed shortly thereafter, at about 71 ms, by an action potential in the LMAN. This last action potential corresponds to the correlation observed by Kimpo *et al.* [2].

Figure 8 explores in a bit more detail what is happening to make the response of the DLM-PN appear so long after the action potential in the SN inhibits AF and releases the DLM-PN. Here we see the burst of five HVc spikes with ISI 2 ms arrive at time 800 ms. In the top panel we show the spikes at 800 ms as well as the activation $m_{DLM}(t)$ and inactivation $h_{DLM}(t)$ variables for the Na channel in the DLM-PN. Because the DLM-PN is hyperpolarized by the inhibitory action of the AF periodic firing, it undergoes a slow recovery before firing an action potential. In the lower panel we show the DLM-PN and LMAN action potentials associated with this burst from HVc arriving at the SN. The time delay ΔT for this event is ≈63 ms.

In Fig. 9 we plot the variation of ΔT as a function of R in our model AFP. It will turn out to be quite important that both positive and negative slopes appear in this result. The positive slopes of $\Delta T(R)$ will be associated with stability in the synaptic plasticity dynamics at the RA. The value of R can be affected by introducing antagonists to the GABA (inhibitory) connections within the DLM. In principle, therfore, one can experimentally explore a curve similar to Fig. 9.

E. The role of inhibition from X→DLM

The inhibition in projections from area X to DLM cells is well established, and if one looks at the overall block dia-

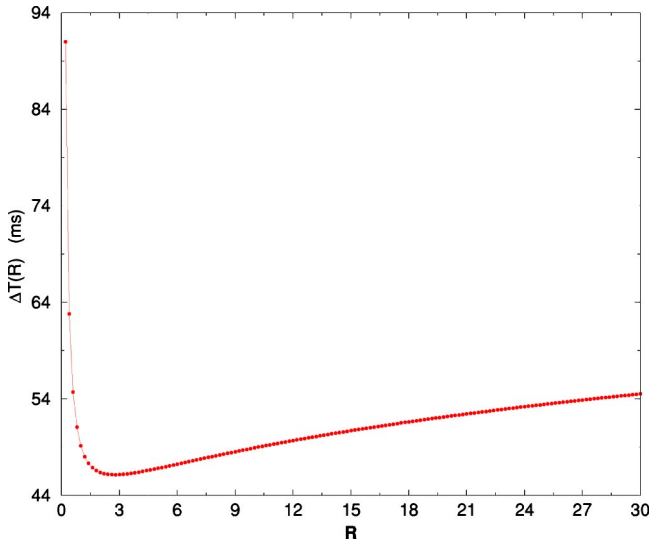

FIG. 9. The time ΔT for a signal to traverse the AFP depends on the strength of the AF→DLM inhibitory connection. The inhibitory conductance relative to a baseline value is the ratio $R = g_{AF\text{-}DLMPN}/g_{AF\text{-}DLMPN\text{-}Baseline}$. Positive slope in $\Delta T(R)$ is associated with stability in RA plasticity by the argument given in the text.

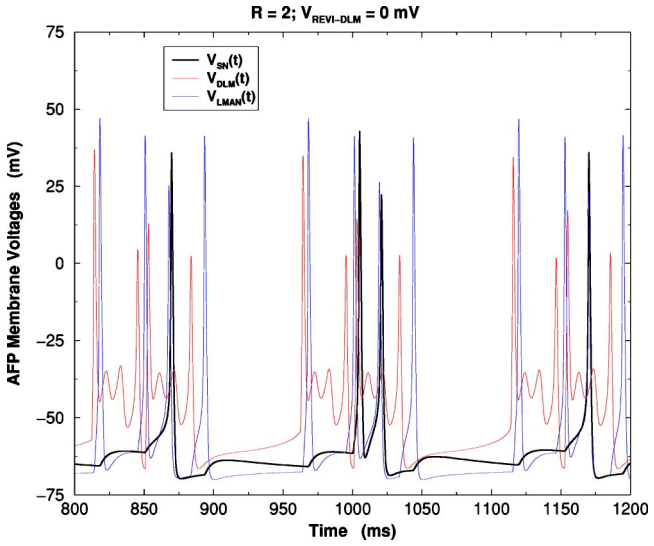

FIG. 10. The AFP output when the synaptic current between the area X output neuron, AF, is changed from inhibitory to excitatory by making $V_{REVI\text{-}DLM}=0$ mV instead of −75 mV. There is a burst of spikes from HVc at 980 ms, but the autonomous firing of the SN and other neurons obscures the identification of ΔT. The RA neuron receives many inputs from the PN in the LMAN which are not associated with an HVc burst because of the oscillations of the AFP loop. In this calculation $R=2$.

gram of the AFP as represented in Fig. 1, we see it is the only internuclear inhibition in the AFP. It is interesting to ask what would happen if we replaced this inhibitory coupling with an excitatory connection. We did that by changing the reversal potential in the AF→DLM connection from −75 mV to 0 mV, leaving all else in the circuit the same. A typical result of this change is seen in Fig. 10 where a burst of five spikes from HVc with ISI 2 ms arrives at area X at t=980 ms. The firing of LMAN-PN, and all the other cells actually, is rather independent of the presence of this innervation from HVc. Clearly, the SN fires immediately upon this innervation from HVc, but the autonomous oscillations preceding the HVc burst continue. The membrane voltage of the AF neuron is not shown, but it exhibits regluar oscillations away from $t=980$ ms.

IV. DYNAMICS WITH COUPLING OF THE RA AND THE AFP

We now have two, as yet unconnected, results on the dynamics of the birdsong system: (1) a time delay of $\Delta T \approx 50$ ms yields a zero in changes in AMPA conductivity at the AMPA receptors on RA neurons using the observed distribution of AMPA and NMDA receptors and a biophysically motivated model of plasticity, and (2) a time delay of $\Delta T \approx 50$ ms arises in a model of the control pathway, the AFP, when various levels of excitation relative to inhibition in the AFP loop are considered.

We now wish to connect these two results. Our proposal for this begins with the question how the RA "knows" that the AFP has selected a relevant time delay ΔT, and equivalently how the AFP "knows" the time delay it has selected has resulted in no further change in synaptic plasticity at the HVc→RA junctions, and thus alteration of the song premotor pathway and thus the song.

A natural solution to this would be a neural connection between RA and the AFP which would feedback this information to each. There is a known, but physiologically unexplored, RA→DLM connection [37–39]. Dave and Margoliash [40] and Luo and Perkel [34] have discussed the role of this RA→DLM connection. Indeed, our attention was drawn to this connection by Perkel [22]. These authors did not develop the conjectures central to our model concerning the detailed RA excitatory connection to the DLM-INs (type II neurons) and then through them via inhibition to the DLM-PNs (type I neurons). Nor did they draw the quantitative conclusions resulting from this connection flowing from our model.

We are not proceeding on solid experimental ground here, but we have explored the possibility that the RA-PNs project excitatory connections to the DLM-INs which then project inhibition to the DLM-PNs. These connections are indicated by the dashed lines in our graphical representation of the various nuclei and the HVc,RA,AFP system. The equations for these connections have all been given in the previous section.

This connection provides the feedback loop required to make the simultaneous determination of $g_{RA}(t)$ and ΔT. We can argue how, qualitatively, this connection might stabilize the coupled system. Suppose the parameters of the system, R and others,are such that if we begin at some initial value of $g_{RA}(t)=g_{RA}(0)$, one burst of HVc arriving directly at the RA and arriving ΔT later via the AFP leads to $\Delta g_{RA}>0$. If this change in Δg_{RA} leads to $\Delta T>0$, namely, the slope $\partial \Delta T/\partial g_{RA}>0$, then looking at Fig. 4, we see that this would

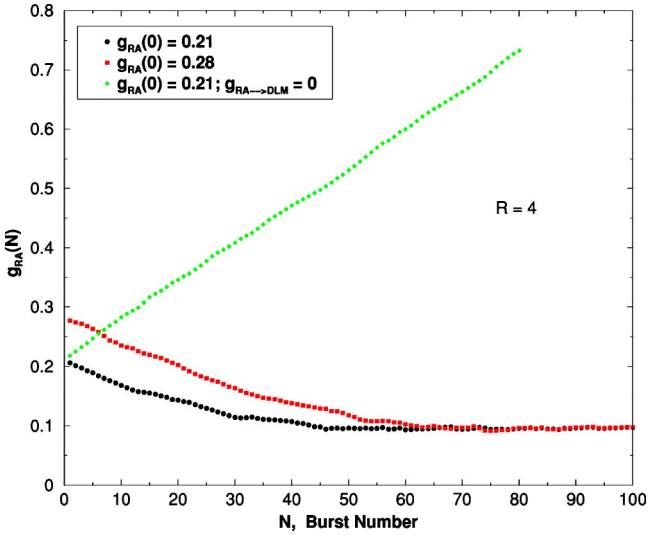

FIG. 11. With $R=4$ we start the coupled HVc,RA,AFP dynamical system at $g_{RA}(0)=0.21$ and then $g_{RA}(0)=0.28$. Each initial condition lies within the same basin of attraction of the map $g_{RA}(N) \rightarrow g_{RA}(N+1)$, determined by presenting many bursts from HVc separated by 2000 ms. We see $g_{RA}(N\rightarrow\infty)\approx 0.095$ and by examining the stable system we find $\Delta T=51.67$ ms. If we turn off the RA$\rightarrow$DLM connection, the map is unstable and $g_{RA}(N)$ grows without bound.

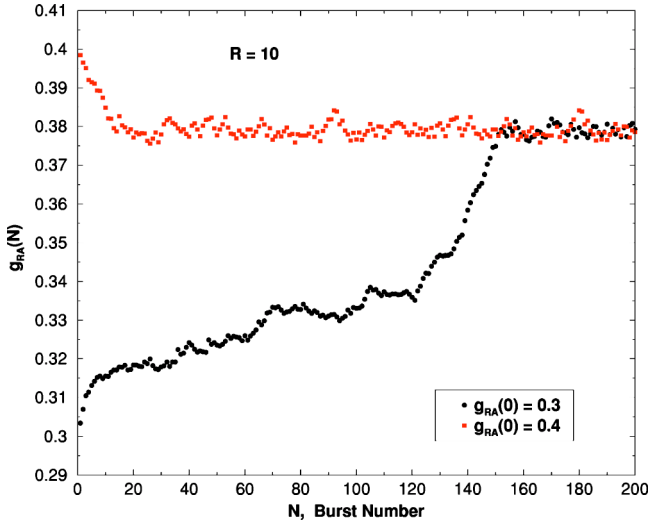

FIG. 12. With $R=10$ we start the coupled HVc,RA,AFP dynamical system at $g_{RA}(0)=0.3$ and then $g_{RA}(0)=0.4$. Each initial condition lies within the same basin of attraction of the map $g_{RA}(N) \rightarrow g_{RA}(N+1)$, determined by presenting many bursts from HVc separated by 2000 ms. We see $g_{RA}(N\rightarrow\infty)\approx 0.038$ and by examining the stable system we find $\Delta T=51.14$ ms. If we turn off the RA$\rightarrow$DLM connection, the map is unstable and $g_{RA}(N)$ grows without bound.

tend to lead to $\Delta g_{RA}<0$, and we might achieve stability. If the slope were opposite at the selected parameter values, the opposite effect would occur, and we might anticipate instability in the coupled system.

The argument couched in terms of the slope $\partial\Delta T/\partial R$ leads to the conclusion that positive values of this slope result in stabilizing changes in Δg_{RA}, while negative slopes lead to instability. Increasing g_{RA} increases the level of *inhibition* in the AFP because the RA connects to the AFP via excitation of a neuron, the DLM-IN, which inhibits the DLM-PN. Thus $\Delta g_{RA}>0$ is approximately equivalent to $\Delta R>0$. The $\Delta T(R)$ relationship for our model shown in Fig. 9 allows for both stable and unstable dynamics of the conductance g_{RA}. If these qualitative arguments are borne out, then by changing AFP parameters, R among them, one might be able to stabilize and destabilize song by using neuromodulators to change such critical ratios.

Our first example selects $R=4$ in the AFP. We then select $g_{RA}(0)$ and present a sequence of HVc bursts comprised of five spikes with ISI 2 ms to both RA and to the SN neuron in area X. Through our synaptic plasticity rule, we evaluate $\Delta g_{RA}(0)$ and, keeping R fixed, change g_{RA} to $g_{RA}(1)=g_{RA}(0)+\Delta g_{RA}(0)$. By presenting a sequence of HVc bursts, labeled by $N=1,2,\ldots$, separated by 2000 ms between bursts, we then define a dynamical map $g_{RA}(N)\rightarrow g_{RA}(N+1)=g_{RA}(N)+\Delta g_{RA}(N)$. Such maps are quite familiar from the study of discrete time dynamical systems.

In Figure 11 we show the outcome of iterating this map for three cases when $R=4$: (1) $g_{RA}(0)=0.21$ with the RA$\rightarrow$DLM-IN connection on, and (2) with that connection turned off. Then we set $g_{RA}(0)=0.28$ and recalculate $g_{RA}(N)$ with the RA$\rightarrow$DLM coupling on. We see that for $R=4$ the dynamical map has a wide basin of attraction within which $g_{RA}(N\rightarrow\infty)\approx 0.095$. This is a stable fixed point of the map, and the associated ΔT as $N\rightarrow\infty$ is 51.67 ms. If we turn off the RA$\rightarrow$DLM connection, these become unstable points for the plasticity dynamics, and from each initial condition, $g_{RA}(N)$ grows without bound. Only the growth from $g_{RA}(0)=0.21$ is shown in the figure.

Next we selected $R=10$ and performed the same set of calculations for $g_{RA}(0)=0.3$ and for $g_{RA}(0)=0.4$. This time $g_{RA}(N\rightarrow\infty)=0.038$ and the associated $\Delta T=51.14$ ms. Again, removing the RA$\rightarrow$DLM connection destabilizes the system. Figure 12 shown $g_{RA}(N)$ when the RA$\rightarrow$DLM connection is on.

Finally, selecting $R=0.2$, where we expect instability from our qualitative arguments, we see in Fig. 13 that $g_{RA}(N)$, starting at $g_{RA}(0)=0.21$, systematically decreases. We have manually cut off this decrease at 0 for biophysical reasons. This could be built into the plasticity model [19]. Other initial conditions $g_{RA}(0)$ over a range of 0.25 to 1.5 behaved the same way at this value of R.

V. SUMMARY AND CONCLUSIONS

We have explored the neural dynamics of the song system as shown in Fig. 1 using anatomical and electrophysiological information about the structure of the neural nuclei in this system and the connections among them. Using observations about the relative amounts of NMDA and AMPA receptors at the RA junctions of HVc and LMAN projections [14], we explored the implications of our biophysical model of synaptic plasticity [15]. This indicated that in response to bursts of spikes from HVc and LMAN separated by ΔT the changes

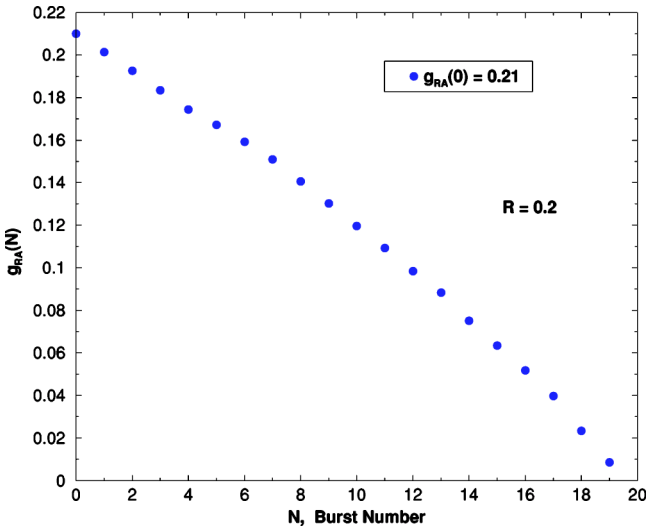

FIG. 13. With $R=0.2$ we start the coupled HVc,RA,AFP dynamical system at $g_{RA}(0)=0.21$. In this case the map $g_{RA}(N) \rightarrow g_{RA}(N+1)$, determined by presenting many bursts from HVc separated by 2000 ms drives $g_{RA}(N)$ to smaller and smaller values. We have had to manually cut off the decrease of $g_{RA}(N)$ by imposing a lower bound of 0. This is not built into the model, but could easily be added [19]. This behavior is seen for all values of $g_{RA}(0)$ we examined for $R_{IE}=0.2$, and our qualitative arguments in the text suggest this should be so.

in AMPA conductivity Δg_{RA} would be zero near 40–50 ms. This is much larger time delay than a similar structure seen in experiments in mammalian cortex and other preparations [18,41] where about 10 ms is appropriate. We attribute this to the specific distribution of NMDA and AMPA receptors at the RA dendrites.

It was very interesting that this time delay $\Delta T \approx 40-50$ ms is also that seen in experiments on correlation between firing in RA and neural activity in the LMAN [2] where two significant peaks were seen: one peak in correlated activity was observed for RA firing about 10 ± 3 ms after LMAN activity, and a second peak where RA is active about 50 ± 10 ms before LMAN activity. The first peak is associated with the known excitatory connection from LMAN to RA [42–44], while the second was identified as coming from common input from HVc directly to the RA and through the AFP. This interpretation was strengthened by the consistency of correlations between HVc and other nuclei in both [2,10] and elsewhere. The results of Kimpo *et al.* [2] are also a strong indication that the nuclei of the song system act in a coherent fashion suggestive of some intranuclear synchronization among the many neurons in each nucleus as well as act coherently in an internuclear manner to propagate timing information from HVc to RA through two paths.

We then inquired into the operation of the AFP effectively as a time delay transfer function conveying information to RA with a delay ΔT. We found that delays of order 40 to 60 ms were produced by treating each nucleus of the AFP as a collection of individual HH model neurons with cell properties known from experiments and synaptic connections as observed. The time delay depended in an interesting manner on the relative inhibitory connection R to the DLM projection neuron.

Within the AFP model we addressed an addtional question: What would happen if the area X→DLM connection were excitatory instead of inhibitory as observed? This is not testable experimentally, but we saw that an excitatory area X→DLM connection leads to regular, apparently autonomous firing of the AFP. This is not consistent with the observations [2] as one might expect.

The plasticity calculations and the AFP time delay calculations, though interesting and quite suggestive, gave no clue how the RA and the AFP communicated ΔT to each other. To accomplish this we noted the existence of a connection between RA and DLM [22,37–39] whose electrophysiological properties are not explored. Using a conjecture on this connection, namely, that the RA projects excitation to the known DLM-IN [34] and in its turn this inhibits the DLM-PN which projects to the LMAN while also receiving input from the AF in the area X nucleus.

Because strengthening the HVc→RA excitatory connections g_{RA} enhances inhibition to the AFP through this conjecture, we anticipated that in regions of $\Delta T(R)$ with positive slope, stability in the plasticity dynamics would be seen. Indeed, we demonstrated this in several examples, and two were presented in Figs. 11 and 12. It is also shown there that removing the RA→DLM connection destabilized the HVc →RA connection as the plasticity rule led to steadily increasing g_{RA} in time measured by the number of HVc bursts, separated by 2000 ms, presented to the RA and to the AFP.

The network structure we have presented is consistent both within itself and with observations [2,12,14,34]. Because it relies on unmeasured properties of the RA→DLM connection it can be checked in a qualitative manner by electrophysiological and pharmacological measurements at that connection. Additionally we have suggested that ΔT in the AFP loop [2] can be directly affected by neuromodulators which alter R and that both positive and negative slopes in the function $\Delta T(R)$ should be present.

This suggests the interesting idea that if the song system uses the connectivity we suggest here, stabilized adult song could be destabilized by neuromodulators. If R is changed from a region where g_{RA} is stable to one where it is unstable, such as we enabled in our model and show in Fig. 13, one could significantly reduce the strength of the HVc→RA couplings and thus significantly alter the song produced because the instructions from HVc to RA to the songbox would have altered. This too has not been seen, but is testable.

In our model we bypassed the origin of sparse signaling from HVc to the RA [10] and let HVc act as a sparse signal generator projecting to both the RA and area X. We also did not address the issue of auditory feedback from the songbox via various pathways back to HVc, and perhaps other song system nuclei. These need to be addressed to achieve a deeper understanding of learning and memory in this neural system, while our results may shed light on how the song is stabilized within this larger picture.

Finally, as noted in our Introduction, we have chosen to significantly simplify the birdsong system by representing each nucleus by at most a few HH model neurons for each observed cell type within the nucleus. Even this simplification leads to the moderately complex model discussed in this paper as each ion channel and synaptic connection has dy-

namics of its own. It is possible that many of the representations of individual neurons could be further simplified, perhaps using FitzHugh-Nagumo two degree of freedom, spiking neurons [46] at many of the nodes of our full network. This could not be done at the DLM projection neuron where the dynamical response of the internal, activation and inactivation, degrees of freedom play an essential role in determining the time delay ΔT in the AFP. We have not explored a further simplifiction of our model in any detail, though replacing the LMAN nucleus, for example, by a simplified spiking neuron would not change our results. We would arrive at a kind of "hybrid" model, however, where a mixture of simplified spiking neurons and biophysically realistic neurons would both play a role. It is not clear yet whether this would provide an interesting representation of the already simplified biological physics of this network. In connecting the dynamics explored here of the coupled premotor and AFP pathways with the mechanisms for the generation of song [11] we may need a much larger network for each nucleus, and then the issue of simplification of the nodes may become essential.

ACKNOWLEDGMENTS

This work was partially supported by the U.S. Department of Energy, Office of Basic Energy Sciences, Division of Engineering and Geosciences, under Grants No. DE-FG03-90ER14138 and No. DE-FG03-96ER14592, by a grant from the National Science Foundation, NSF Grant No. PHY0097134, by a grant from the Army Research Office, Grant No. DAAD19-01-1-0026, by a grant from the Office of Naval Research, Grant No. N00014-00-1-0181, and by a grant from the National Institutes of Health, NIH Grant No. R01 NS40110-01A2. G.B.M. was partially supported by UBA, Fundacion Antorchas. H.D.I.A. and S.T. were partially supported through the National Science Foundation Physics Frontier Center for Theoretical Biological Physics at UCSD. We enjoyed significant constructive input from Allison Doupe and Michael Brainard at UC San Francisco and from David Perkel of the University of Washington. Comments from M. Fee of MIT were also quite helpful.

APPENDIX

The various constants appearing in the single-compartment Hodgkin-Huxley (HH) type model neurons, the synaptic currents, and our synaptic plasticity model are described here.

1. RA projection neurons

The kinetics of activation and inactivation of sodium and potassium currents in our model of RA neurons were modified from a model of hippocampal pyramidal neurons [45]. We have used faster kinetics to emulate the spiking behavior of RA projection neurons, in response to synaptic input from HVc neurons. The following are the parameters used for the HH type model used for RA projection neurons: $C_M = 1\ \mu\mathrm{F/cm^2}$, $g_{Na} = 215\ \mathrm{mS/cm^2}$, $g_K = 43\ \mathrm{mS/cm^2}$, $g_L = 0.83\ \mathrm{mS/cm^2}$, $E_L = -65$ mV, $E_{Na} = 50$ mV, and $E_K = -95$ mV. NMDA currents of the synapses from HVc and LMAN were two-component models which reproduce the observed fast and slow decay times as seen by Stark and Perkel [14]. $g_N = 0.75\ \mathrm{mS/cm^2}$ represents the strength of the NMDA synapse from HVc onto the RA which is ten times the strength of the NMDA synapse onto the RA from LMAN. The percentage contributions of the fast NMDA component of the synaptic connections from HVc and LMAN were $w_{HVc} = 0.21$ and $w_{LMAN} = 0.41$, respectively. The fast and slow NMDA decay time constants of the synaptic connections from HVc were $\tau_{N1\text{-}HVc} = 19.75$ ms and $\tau_{N2\text{-}HVc} = 99.75$ ms, respectively; while those for synaptic connections from LMAN were $\tau_{N1\text{-}LMAN} = 29$ ms and $\tau_{N2\text{-}LMAN} = 139$ ms. The constants characterizing rise times for the two NMDA components for the HVc to RA synapse were $S_{N1\text{-}HVc} = 20/19.75$ and $S_{N2\text{-}HVc} = 100/99.75$, while for the LMAN to RA synapse they were $S_{N1\text{-}LMAN} = 30/29$ and $S_{N2\text{-}LMAN} = 140/139$. The extracellular magnesium concentration was chosen to be $[Mg^{2+}] = 1$ mM which is a standard value [46]. The maximal conductance and reversal potential of the inhibitory GABAergic synaptic connections from RA interneurons were $g_{RA\text{-}IN} = 15\ \mathrm{mS/cm^2}$ and $E_{revI} = -80$ mV. Weak coupling between the RA projection neurons was characterized by $g_{RA\text{-}PN} = 0.05\ \mathrm{mS/cm^2}$ representing the fact that spontaneous oscillatory behavior of RA projection neurons is unsynchronized. The dc currents $I_{DC\text{-}PN1} = I_{DC\text{-}PN2} = 1.93\ \mu\mathrm{A/cm^2}$ were required to obtain the approximately 20 Hz spontaneous spiking behavior observed in RA projection neurons.

2. RA interneurons

The passive and active membrane parameters of the RA interneuron were the same as those of RA projection neurons: $C_M = 1\ \mu\mathrm{F/cm^2}$, $g_{Na} = 215\ \mathrm{mS/cm^2}$, $g_K = 43\ \mathrm{mS/cm^2}$, $g_L = 0.83\ \mathrm{mS/cm^2}$, $E_L = -65$ mV, $E_{Na} = 50$ mV, $E_K = -95$ mV, $w_{HVc} = 0.21$, $w_{LMAN} = 0.41$, $\tau_{N1\text{-}HVc} = 19.75$ ms, $\tau_{N2\text{-}HVc} = 99.75$ ms, $\tau_{N1\text{-}LMAN} = 29$ ms, $\tau_{N2\text{-}LMAN} = 139$ ms, $S_{N1\text{-}HVc} = 20/19.75$, $S_{N2\text{-}HVc} = 100/99.75$, $S_{N1\text{-}LMAN} = 30/29$, $S_{N2\text{-}LMAN} = 130/129$, and $[Mg^{2+}] = 1$ mM. The maximal conductance of the synaptic connections from the RA projection neurons on to the interneurons was $g_{PNj\text{-}IN} = 0.01\ \mathrm{mS/cm^2}$. The injected dc current was $I_{DC\text{-}RAIN} = 1.6\ \mu\mathrm{A/cm^2}$; this is below threshold for spontaneous oscillations of these RA-INs.

3. Area X spiny neurons SN

The kinetics of activation and inactivation of the sodium and potassium currents in our model of area X spiny neurons and other AFP neurons were those of Hodgkin and Huxley [46]. The following parameters were used for the HH model used to describe area X spiny neurons: $C_M = 1\ \mu F/\mathrm{cm^2}$, $g_{\mathrm{Na}} = 20\ \mathrm{mS/cm^2}$, $g_{\mathrm{K}} = 6.2\ \mathrm{mS/cm^2}$, $g_L = 0.03\ \mathrm{mS/cm^2}$, $E_L = -49.4$ mV, $E_{\mathrm{Na}} = 50$ mV, $E_{\mathrm{K}} = -99$ mV. The maximal conductances of the synaptic connection from HVc and LMAN were $g_{HVc\text{-}SN} = g_{LMAN\text{-}SN} = 0.4\ \mathrm{mS/cm^2}$. These are adjusted so a spike in HVc/LMAN is propagated to the SN with delay of the order of 3–5 ms. The injected dc current was $I_{DC\text{-}SN} = -0.55\ \mu A/\mathrm{cm^2}$; this is below threshold for oscillation.

4. Area X aspiny fast firing neurons AF

The passive and active membrane parameters of the HH model representing AF neurons were the same as those for SN neurons: $C_M=1\ \mu\mathrm{F/cm^2}$, $g_{\mathrm{Na}}=20\ \mathrm{mS/cm^2}$, $g_{\mathrm{K}}=6.2\ \mathrm{mS/cm^2}$, $g_L=0.03\ \mathrm{mS/cm^2}$, $E_L=-49.4\ \mathrm{mV}$, $E_{\mathrm{Na}}=50\ \mathrm{mV}$, $E_{\mathrm{K}}=-99\ \mathrm{mV}$. The dc, current $I_{DC\text{-}AF}=-0.146\ \mu\mathrm{A/cm^2}$ was adjusted so the AF neuron spontaneously spikes at about 20 Hz. The maximal conductance of the GABAergic synaptic connection from the SN was $g_{SN\text{-}AF}=g_I\ \mathrm{mS/cm^2}$, where $g_I=g_E R_{IE}$, $g_E=0.4\ \mathrm{mS/cm^2}$, and R_{IE} varies as indicated in the text.

5. Type I DLM neuron, DLM-PN

The passive parameters and sodium and potassium currents of the type I DLM neuron were the same as those of other AFP neurons: $C_M=1\ \mu\mathrm{F/cm^2}$, $g_{\mathrm{Na}}=20\ \mathrm{mS/cm^2}$, $g_{\mathrm{K}}=6.2\ \mathrm{mS/cm^2}$, $g_L=0.03\ \mathrm{mS/cm^2}$, $E_L=-49.4\ \mathrm{mV}$, $E_{\mathrm{Na}}=50\ \mathrm{mV}$, and $E_{\mathrm{K}}=-99\ \mathrm{mV}$. In addition, these neurons contain the hyperpolarization-activated current I_h and the low threshold Ca^{2+} current I_T. The maximal conductances of I_h and I_T were chosen as $g_h=0.045\ \mathrm{mS/cm^2}$ and $g_T=3.775\times10^{-5}\ \mathrm{mS/cm^2}$, respectively. The equilibrium ratio of extracellular to intracellular calcium was taken to be $[Ca^{2+}]_o/[Ca^{2+}]_i=40\,000$ [23]. The maximal conductance of the GABAergic synaptic connection from the type II DLM neuron was $g_{DLMIN\text{-}DLMPN}=4.0\ \mathrm{mS/cm^2}$, and the maximal conductance of the GABAergic synaptic connection from the AF was $g_{AF\text{-}DLMPN}=g_I\ \mathrm{mS/cm^2}$, where $g_I=g_E R_{IE}$, $g_E=0.4\ \mathrm{mS/cm^2}$, and R_{IE} varies as indicated in the text.

6. Type II DLM neuron, DLM-IN

The passive and active membrane parameters of the type II DLM neuron were the same as those of spiny, AF, and LMAN neurons: $C_M=1\ \mu\mathrm{F/cm^2}$, $g_{\mathrm{Na}}=20\ \mathrm{mS/cm^2}$, $g_{\mathrm{K}}=6.2\ \mathrm{mS/cm^2}$, $g_L=0.03\ \mathrm{mS/cm^2}$, $E_L=-49.4\ \mathrm{mV}$, $E_{\mathrm{Na}}=50\ \mathrm{mV}$, and $E_{\mathrm{K}}=-99\ \mathrm{mV}$. The injected dc current was $I_{DC\text{-}AF}=-0.55\ \mu\mathrm{A/cm^2}$. The maximal conductance of the synaptic connections from the RA projection neurons was $g_{RA\text{-}DLMIN}=4.0\ \mathrm{mS/cm^2}$. The value of this coupling term was chosen so activity changes in the RA projection neurons are rapidly transmitted to DLM type II inhibitory neurons through the excitatory coupling.

7. LMAN neuron

The role for the LMAN in this model is just to act as a relay neuron transmitting the response of DLM firing timings back to the RA as output of the AFP loop. The parameters of the HH model for the LMAN are the same as those used for other AFP neurons: $C_M=1\ \mu\mathrm{F/cm^2}$, $g_{\mathrm{Na}}=20\ \mathrm{mS/cm^2}$, $g_{\mathrm{K}}=6.2\ \mathrm{mS/cm^2}$, $g_L=0.03\ \mathrm{mS/cm^2}$, $E_L=-49.4\ \mathrm{mV}$, $E_{\mathrm{Na}}=50\ \mathrm{mV}$, and $E_{\mathrm{K}}=-99\ \mathrm{mV}$. The injected dc current was $I_{DC\text{-}LMAN}=-0.55\ \mu\mathrm{A/cm^2}$, while the maximal conductance of the synaptic connections from the type I DLM neuron was $g_{DLMPN\text{-}LMAN}=0.04\ \mathrm{mS/cm^2}$.

8. Synaptic plasticity model

Our model of synaptic plasticity at HVc-RA synapses was the same model we have used previously [15]. The intracellular Ca^{2+} concentration was scaled to the equilibrium resting value $C_0=100$ nM, for convenience. The Ca^{2+} decay time constant was set to $\tau_C=28$ ms, rather than 80 ms as in our earlier paper, to better approximate recent experimental data [47]. The parameters of our plasticity model were taken from our earlier results [15]: the decay time constants for our phenomenological variables $P(t)$ and $D(t)$ were $\tau_P=10$ ms and $\tau_D=30$ ms, respectively. The constants in the driving functions of $P(t)$ and $D(t)$ are $L=4$, $M=8$, and $\xi=6.75$. The constants in our nonlinear competition between $P(t)$ and $D(t)$ were $\gamma=1$ and $\eta=4$. The constants controlling the influx of Ca^{2+} through NMDA and AMPA receptors at the HVc-RA synapses were $g_{NC}=0.057\ \mathrm{mV^{-1}}$ and $g_{AC}=10^{-6}\ \mathrm{mV^{-1}}$, respectively.

[1] A. J. Doupe and P. K. Kuhl, Annu. Rev. Neurosci. **22**, 567 (1999).
[2] R. R. Kimpo, F. E. Theunissen, and A. J. Doupe, J. Neurosci. **23**, 5750 (2003).
[3] R. Laje and G. B. Mindlin, Phys. Rev. Lett. **89**, 288102 (2002).
[4] G. B. Mindlin, T. J. Gardner, F. Goller, and R. Suthers, Phys. Rev. E **68**, 041908 (2003).
[5] R. Mooney, M. J. Rosen, and C. B. Sturdy, J. Comp. Physiol. [A] **188**, 879 (2002).
[6] E. A. Brenowitz, D. Margoliash, and K. W. Nordeen, J. Neurobiol. **33**, 495 (1997).
[7] D. Margoliash, J. Comp. Physiol. [A] **188**, 851 (2002).
[8] M. S. Brainard and A. J. Doupe, Nature (London) **417**, 351 (2002).
[9] M. S. Brainard and A. J. Doupe, Nature (London) **404**, 762 (2000).
[10] R. H. R. Hahnloser, A. A. Kozhevnikov, and M. S. Fee, Nature (London) **419**, 65 (2002).
[11] H. D. I. Abarbanel, L. Gibb, G. Mindlin, and S. Talathi, J. Neurophysiol. **92**, 96 (2004).
[12] J. E. Spiro, M. B. Dalva, and R. J. Mooney, J. Neurophysiol. **81**, 3007 (1999).
[13] A. C. Yu and D. Margoliash, Science **273**, 1871 (1996).
[14] L. L. Stark and D. J. Perkel, J. Neurosci. **19**, 9107 (1999).
[15] H. D. I. Abarbanel, L. Gibb, R. Huerta, and M. I. Rabinovich, Biol. Cybern. **89**, 214 (2003).
[16] L. Ding and D. J. Perkel, J. Neurosci. **22**, 5210 (2002); **22**, 6835 (2002).
[17] L. Ding, D. J. Perkel, and M. A. Farries, J. Neurosci. **23**, 6086 (2003).
[18] G-Q. Bi and M-m Poo, Annu. Rev. Neurosci. **24**, 139 (2001).
[19] T. Nowotny, M. I. Rabinovich, and H. D. I. Abarbanel, Phys. Rev. E **68**, 011908 (2003).
[20] R. C. Malenka and R. A. Nicoll, Science **285**, 1870 (1999).
[21] R. Malinow and R. C. Malenka, Annu. Rev. Neurosci. **25**, 103

(2002).
[22] D. J. Perkel (private communication).
[23] B. Hille, *Ion Channels of Excitable Membranes*, 3rd ed. (Sinauer Associates, Sunderland, MA, 2001).
[24] L. Nowak, P. Bregestovski, P. Ascher, A. Hebet, and A. Prochiantz, Nature (London) **307**, 462 (1984).
[25] S. N. Yang, Y. G. Tang, and R. S. Zucker, J. Neurophysiol. **81**, 781 (1999).
[26] A. M. Zhabotinsky, Biophys. J. **79**, 2211 (2000).
[27] T. V. Bliss and T. Lomo, J. Physiol. (London) **232**, 331 (1973); T. Lomo, Philos. Trans. R. Soc. London, Ser. B **358**, 617 (2003).
[28] R. Malinow and J. P. Miller, Nature (London) **320**, 529 (1986).
[29] M. A. Farries and D. J. Perkel, J. Neurophysiol. **84**, 2502 (2000).
[30] M. A. Farries and D. J. Perkel, J. Neurosci. **22**, 3776 (2002).
[31] M. Luo and D. J. Perkel, J. Comp. Neurol. **403**, 68 (1999).
[32] M. Luo and D. J. Perkel, J. Neurosci. **19**, 6700 (1999).
[33] M. Luo, L. Ding, and D. J. Perkel, J. Neurosci. **21**, 6836 (2001).
[34] M. Luo and D. J. Perkel, J. Neurophysiol. **88**, 1903 (2002).
[35] D. A. McCormick and H. C. Pape, J. Physiol. (London) **431**, 291 (1990).
[36] D. A. McCormick and J. R. Huguenard, J. Neurophysiol. **68**, 1384 (1992).
[37] D. S. Vicario, NeuroReport **4**, 983 (1993).
[38] J. M. Wild, J. Comp. Neurol. **338**, 225 (1993).
[39] G. E. Vates, D. S. Vicario, and F. Nottebaum, J. Comp. Neurol. **380**, 275 (1997).
[40] A. S. Dave and D. Margoliash, Science **290**, 812 (2000).
[41] M. Nishiyama, K. Hong, K. Mikoshiba, M.-m. Poo, and K. Kato, Nature (London) **408**, 584 (2000).
[42] S. Okuhata and N. Saito, Brain Res. Bull. **18**, 35 (1987).
[43] R. Mooney, J. Neurosci. **12**, 2464 (1992).
[44] S. W. Bottjer, K. A. Halsema, S. A. Brown, and E. A. Miesner, J. Comp. Neurol. **279**, 312 (1989).
[45] R. D. Traub and R. Miles, *Neuronal Networks of the Hippocampus* (Cambridge University Press, Cambridge, 1991), Appendix.
[46] C. Koch, *Biophysics of Computation: Information Processing in Single Neurons* (Oxford University Press, New York, 1999).
[47] B. L. Sabatini, T. G. Oertner, and K. Svoboda, Neuron **33**, 439 (2002).